# Tunable Gamma-Rays in a Thermal Fission Environment for Microelectronics Testing

M. Niichel & S. Chatzidakis

***Abstract*—Radiation testing of microelectronics is essential for systems operating in space or nuclear environments, but it is both time-intensive and costly. Qualification as a radiation-hardened system by the United States Government typically requires exposure to 50–2000 Rad(Si)/s total dose rate of Co-60 and 1 MeV-equivalent neutron fluence. Domestic testing capacity cannot meet current demand, with some facilities booked up to two years in advance. Early-stage designs frequently fail initial testing, necessitating redesigns that further extend development timelines.**

**This work proposes a new method to produce gamma-rays with tunable energy in a thermal fission environment and allow the use of easier to access low power thermal research reactors to provide earlier, lower-cost radiation screening during the design process. We investigate the use of test casings composed of pure metals or metal-paraffin composites for tuning the thermal fission neutron spectrum to maximize gamma production through carefully selected (n,γ) reactions. The method is verified using high-fidelity MCNP6.3 simulations to model these casings and evaluate dose deposition in silicon within the Purdue University Reactor Number One (PUR-1). Materials such as copper, indium, and cadmium in sheet form and suspended in paraffin wax were found to increase gamma energy deposition in silicon by up to 105% relative to the control PUR-1 fission spectrum. These results support the development of a physical irradiation experiment at PUR-1 to validate the Monte Carlo predictions.**

***Index Terms*—Radiation testing, Total ionizing dose, Neutron spectrum tailoring, Gamma production, MCNP6.3, PUR-1 reactor, Radiation-hardened electronics, Gamma dose enhancement**

## I. Introduction

One of the challenges associated with designing radiation-hardened systems is the qualification of the part itself. After the divestment of radiation testing facilities following 1991, there was not much demand for commercial hardness assurance testing until the mid-2010s when both nuclear power and space-based assets started becoming mainstream once more [1]. A joint-agency commissioned report determined that the 2030 domestic demand for radiation assurance testing will far exceed the capacity [1]. As a result, emphasis must be placed on alternative testing methods to alleviate the stressed industry.

While planning for radiation testing of an STM32-based system in accordance with the Department of War's (DoW) MIL-STD-750D/883E neutron and total ionizing dose (TID) standards, we found that scheduling a facility that met the timeline or the experimental setup was difficult [2]. As an example, the Co-60 irradiator located at Purdue University was approaching 30 years-old and could not meet the 50-2000 Rad(Si)/s for TID, while several other facilities near the University did not have an irradiator that could accommodate cables for live-monitoring. Efforts to use the White Sands Missile Range Fast Burst Reactor were rendered futile due to scheduling booked out for up to two-years, and the cost of a test approached nearly $200,000 per week. Given that the design was comprised of only commercial parts, it was unknown if any of the components had any resistance to radiation damage. It was suggested to conduct lower-level radiation testing in the Purdue subcritical pile and PUR-1 10 kW research reactor to determine if more rigorous testing was warranted. While the neutron flux in the subcritical pile was ultimately deemed too low, PUR-1 offered a more useful fission environment [3]. In an effort to tailor the highly thermalized PUR-1 neutron flux closer to the 1 MeV equivalent fluence, a 1-mm thick 3N cadmium shield was placed around the device under test (DUT). The results were compared the DUT in the control PUR-1 environment and the MIL-STD Co-60 environment. We observed that the response of the DUT was more in line with the Co-60 testing than the bare PUR-1 environment suggesting a strong dependence on TID [4]. This work suggested that the capture gammas from the Cd-113(n,γ)Cd-114 reaction increased the gamma dose rate relative to the bare environment. This was further supported by TLD measurements [4], [5].

This observation suggests that it may be possible to use materials with a high affinity for neutrons to tune the energy of gammas such that their interaction with silicon-based microelectronics is optimal for any given neutron source. Although, this type of testing will not replace the current hardness assurance threshold, it may be used as an accessible and cost-effective supplement for low-level testing earlier in the microelectronic design process. In this work, we investigate and identify optimal combinations of neutron absorption prompt gamma activation materials to tune the gamma rays in a thermal fission environment. We verify the validity of the method through the use of MCNP6.3 and propose experiments to generate results through metal foil activation in line with ASTM E262-17 and lithium-fluoride (LiF) TLD 600/700 measurements in line with ATSM E668-20 [6],[7].

M. Niichel is a first-lieutenant with the United States Space Force and Air Force Institute of Technology's Civilian Institute at Purdue University, West Lafayette, IN 47907 USA (e-mail: matthew.niichel@spaceforce.mil).

S. Chatzidakis, PhD is an assistant professor at the school of nuclear engineering, Purdue University, West Lafayette, IN 47907 USA (email: schatzid@purdue.edu).

## II. Background

The National Ignition Facility coequally known as NIF is one of many domestic efforts for developing the viable use of fusion technology. Their facility hosts numerous sub-facilities that conduct nuclear experiments. Where one such experiment, is the ATHENA energy tuning assembly. A chamber with specifically designed material composition for down scattering fusion neutrons into a thermonuclear plus prompt fission neutron spectrum [8]. This particular radiation environment is the basis of the Co-60 and 1-MeV equivalent fluence requirement of the military standard for testing microelectronics [9],[10].

A PhD dissertation in 2017 out of UC Berkely discusses the development of the ATHENA facility. Bevins describes the use of MCNP to narrow down material section. Then presents foil activation kits containing various metals and the subsequent use of Pacific Northwest National Laboratory's STAYSL code for neutron spectrum unfolding. The result of the dissertation provides a recommendation for material composition for the ATHENA at the NIF [11].

The Air Force Institute of Technology has made use of ATHENA as recently as 2022 for conducting microelectronic survivability tests on transistor technologies. In Kloppenburg's report, he compares the damage of the 2N2222 bipolar transistor (BJT) between the Ohio State Research reactor OSURR and the ATHENA facility at NIF. The hypothesis states that the post-irradiation measurements of the BJT will be the same regardless of neutron energy, but the dynamic measurements during irradiation will vary due to different damage mechanisms. Evidence in support of the hypothesis is presented in the thesis showing that post-irradiation effects are independent of neutron energy, however dynamic measurements are not [12]. It is mentioned that gamma rays were not considered in this work, for either the reactor or ATHENA.

A contradiction from Kloppenburg was noted by work conducted by Niichel *et al.* when testing the BSS119N MOSFET in PUR-1. Niichel's work makes an attempt to classify the effects of gamma rays and neutrons separately [4]. Evidence suggests that the energy of the neutrons does affect the post-irradiation effects by shifting the threshold voltages of the MOSFET. It was proposed that thermal neutrons induced activations internal to the device, ultimately delivering additional TID. Whereas, epithermal neutrons did not induce the same level of activation. This report aims to further investigate the effects that thermal neutron induced gammas on a DUT, and maximize the effect for radiation testing.

## III. Material Selection

The selection of the material followed four categories in order of precedence. First, the material must have a relatively large microscopic cross-section for the (n, γ) reaction. Second, if the material did not provide a prompt gamma, the half-life of the isotope must be small compared to the irradiation time to allow for build-up to occur. Third, the material should provide a high energy gamma, such that attenuation in most materials is unlikely. Finally, the material needed to be accessible.

The intention of these criteria is to build a composite shield that maximizes the energy width of the incident neutrons, while producing a useful energy and quantity of photons from the interaction. The selected materials for the design of the energy tuning include copper, indium, and cadmium. By combining the metals in order of increasing cross-section, the effective energy range of the composite may increase. However, the reverse may also cause an adverse effect on gamma production due to the combination of spectrum hardening and gamma attenuation. Equations (1)-(5) provide a simplified expression used to validate the claim where there are two energy groups of neutrons fast $\Phi_F$ and thermal $\Phi_T$.

$$\Phi_{out} = M_n M_{n+1} \dots M_{n+m} \Phi_{in} \tag{1}$$

$$\Phi_{in} = \begin{pmatrix} \Phi_F \\ \Phi_T \end{pmatrix} \tag{2}$$

$$M_n = \begin{pmatrix} M_{F\to F} & M_{F\to T} \\ M_{T\to F} & M_{T\to T} \end{pmatrix} \tag{3}$$

$$M_n = \begin{pmatrix} e^{-\Sigma_{T_F} t} & 1 - e^{-\Sigma_{T_T} t} \\ 1 - e^{-\Sigma_{T_F} t} & e^{-\Sigma_{T_T} t} \end{pmatrix} \tag{4}$$

$$H = \frac{\Phi_{out}}{\Phi_{in}} \tag{5}$$

Where, the hardness parameter $H$ is the change in the spectrum hardness for any layer $n$, up to $m$ number of layers. For any given order of layers, the hardness parameter varies. The value of the hardness parameter at the effluent side of one layer modifies the total macroscopic cross-section for interaction $\Sigma_T$ on the influent side of the subsequent layer. Computing this analytically, is challenging enough assuming 1 MeV and 0.025 eV neutrons. However, the complication of epithermal resonances and secondary reactions complicates the solution. Thus, indicating that Monte Carlo Methods are better suited for such computations.

The ENDF/B-VIII.0 cross-section library is used to provide the data for selected materials. However, for metals like copper where there are two isotopes that have a high affinity for neutrons, a combined data set can be generated by summing the isotope indices together as a function of incident neutron energy. While cadmium has several stable isotopes, the cross-section for Cd-113 is four-orders of magnitude larger than the other isotopes, and is therefore the dominating effect. Indium also has two stable isotopes, with a similar cross-section, however In-113 has an abundance of less than 5%. Therefore, the effect is strongly correlated to In-115. Finally, copper has two isotopes with similar cross-sections, but the Cu-63 and Cu-65 abundance are 69.2% and 30.9% respectively. Therefore, both must be considered. The cross-section data for Cd-113, In-115, and Cu-63/65 are plotted in Fig. 1. Although, all of these isotopes subsequently decay into other materials, the timeline of the test is small compared to the buildup of other isotopes, thus they can be neglected.

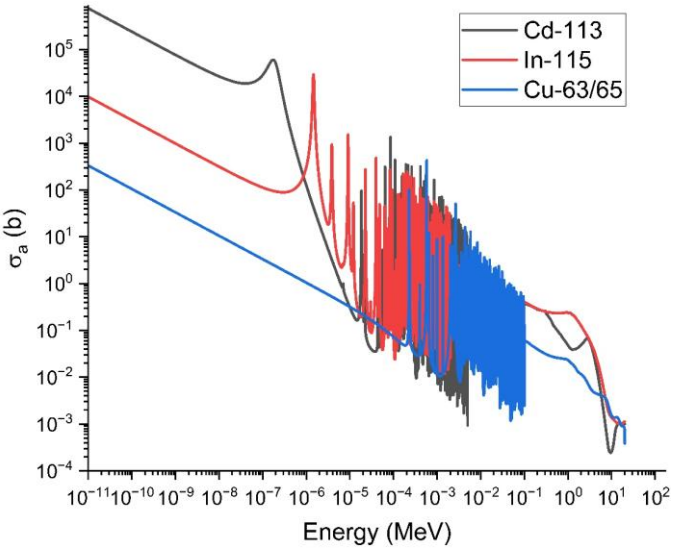


Fig. 1 ENDF/VIII.0 microscopic cross-section for absorption and production of gamma energy of selected metals as a function of energy [13], [14], [15], [16].

## IV. Modeling and Simulation

The Purdue research reactor is 10 kW pool type core loaded with low-enriched uranium-235 [17]. The work conducted by Miller *et al.* and Townsend, provide in detail the dimensions and characteristics for the reactor and auxiliary equipment [17], [18]. Furthermore, there exists a 7.62 cm diameter high-density polyethylene drop tube located 30.00 cm from the core that extends the entire depth of the water pool. It is with this information that the MCNP6.3 geometry can be established for the experimental setup of the energy tuning experiments. Fig. 2 provides a simplified geometry of the PUR-1 pool and core used for modeling the radiation environment.

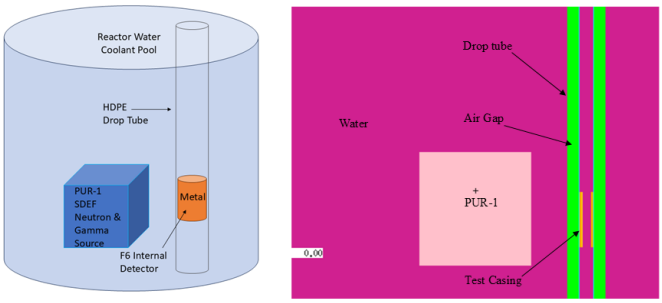


Fig. 2 Simplified input geometry of the PUR-1 Reactor and the drop tube with device under test compared with MCNP6.3 rendering.

Ultimately, the region of interest in the geometry exists within the drop tube centerline with the core. As a result, the core can be treated as a homogenous rectangular parallelepiped of aluminum and the fission environment can be established with a MCNP SDEF card for irradiation. The particle energy and probabilities for U-235 fission can be found in a Lawerence-Livermore report from 2010 [19]. While the specific fuel composition of PUR-1 remains different from pure U-235, it is assumed that the energy spectrum for neutrons and gammas remain unaffected. The normalized neutron lethargy (ranging from $5.50\times10^{-10}$ – $1.85\times10^{1}$ MeV) at the boundary of the core and the pool interface is displayed in Fig. 3 and the normalized gamma distribution is displayed in Fig. 4.

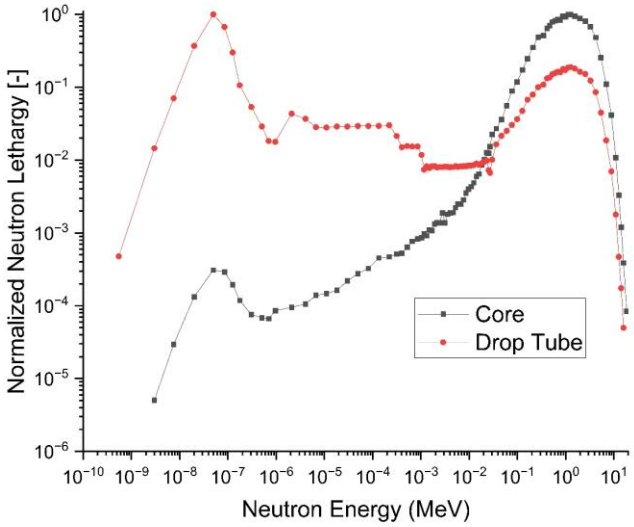


Fig. 3 Comparison of neutron energy spectra at the core boundary an in the center of the drop tube within PUR-1.

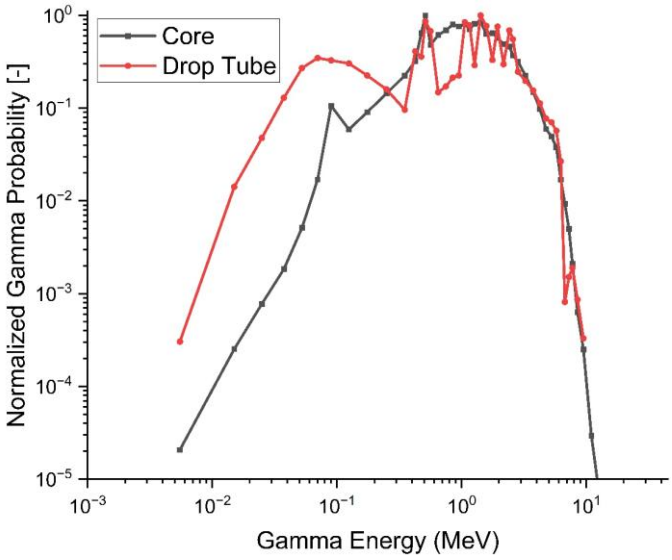


Fig. 4 Comparison of gamma energy spectra at the core boundary an in the center of the drop tube within PUR-1.

The energy tuning material is to be placed internal to a polylactic acid 3D printed capsule of 1.27 cm thickness for the purpose of containing activated materials and for ensuring that parts to be irradiated are easily placed/removed from the drop tube during experiments. One challenge that currently exists is that the 3D printing filament uses pigments that are not strongly regulated. The chemical composition of pigment ranges between 1-3% wt., and can have metal compounds ranging from iron to uranium [20]. Without a chemical analysis, we assume that the color black contains carbon and red/orange are various compositions of iron oxide. In an experimental setup, consistently should be maintained among various filament colors for the drop tube capsules. This will help prevent unsuspecting material activation, but future work may be warranted in the filament itself [21].

The neutron spectrum at the boundary of the pool and the core is only important for the definition of the geometry and the SDEF card in MCNP, as the pool produces a significantly moderated spectrum at the testing location when compared to

the fission energies. Thus, for testing and dosimetry considerations, the neutron spectrum that is present at the center of the drop tube may be used for material selection and as the controlled environment.

The benefit of using Monte-Carlo methods allows for the full consideration of the cross-sections and energy spectrum of the materials without conducting complete integrals. A simple analytical solution can be achieved using the following equations (6)-(10) and assumptions: All neutrons are 0.025 eV, the thickness of each foil layer is 1 mm, gamma-self shielding is neglected, unidirectional neutron travel, and Bragg-Gray cavity theory [22]. A more in-depth procedure for determining the optimal depth is provided below in section VII.

$$\phi_{n,i} = \phi_{n,0} \times exp(-\sum_{j=1}^{i-1} \Sigma_{t,j} \times t_j) \quad (6)$$

$$r_i = \Sigma_{a,i}\phi_{n,i} = N_i\sigma_{a,i}\phi_{n,i} \quad (7)$$

$$\phi_{\gamma,i} = r_i t_i \nu_{\gamma,i} exp[\sum_{k=i+1}^{M}(-\mu_k t_k)] \quad (8)$$

$$\dot{\psi}_{E,i} = \phi_{\gamma,i} E^{(j)}{}_{\gamma,i} \quad (9)$$

$$\dot{D} = 1000 \times \frac{\mu_{en}}{\rho} \times [\sum_{i=1}^{M} \dot{\psi}_{E,i}] \quad (10)$$

Where, $\phi$ is particle flux, $\Sigma_t$ is the total macroscopic cross-section for interaction, $\Sigma_a$ absorption macroscopic cross-section for interaction, $t$ is the material thickness, $N$ is the number of atoms, $\nu_\gamma$ is the gamma branching ratio, μ is the linear attenuation coefficient, $E$ is the gamma energy, $\dot{\psi}_{E,i}$ is the gamma flux, $\mu_{en}/\rho$ is the energy mass attenuation coefficient, and $\dot{D}$ is the dose rate. It is critical to note, that these are a gross-oversimplification of the problem. However, the use of equations (6)-(10) identified the effect of shelf-shielding due to the thickness of the metal sheets.

In an effort to maximize the neutron flux available for metallic capture, it was proposed to suspend the selected metals within a strong thermalizing medium. The use of paraffin wax allows for liquification, mixing, and solidification to any shape that is desired. Density of the metals presents a challenge with generating a homogenous liquid wax and metal product, but the use of fine powdered metals reduces the probability that the metals will migrate to the bottom of the form used to solidify the wax. A 20% by weight fraction was selected subjectively on cost of fine mesh power costs for cadmium an indium. While the concentration of metal may be increased based on literature up near 90% wt. depending on the particle size and density, the value selected for this study is based on practical concerns [23].

Unlike the metal sheets, the wax can be made to any thickness. However, translating the limited volume available in PUR-1 drop tube to the MCNP geometry allows for an approximate thickness of 5.08 cm with a void diameter of 2.54 cm for the DUT. These values are specific to the drop tube diameter of 7.62 cm, and can be modified should this experiment be translated to another facility. The neutron thermalization length for paraffin wax is around 11 cm for an Am-Be neutron source [24]. However, it is important to note that the location of the DUT in PUR-1 experiences a significant portion of thermal neutrons, as a result, there may be a diminishing return on neutrons for a larger thickness of wax.

## V. MCNP Spectrum Results

By applying 1-mm thick sheets to the geometry of the MCNP input, and applying an F4 tally for neutrons and photons at the center of the testing location (material set to silicon), insight to the shift in both energy spectra could be compared to the control shown in Fig. 3 and Fig. 4. This comparison for the materials selected are shown for gamma in Fig. 5 and neutrons in Fig. 6, respectively. The MCNP generated gamma and neutron spectra for the wax models are compared to the control in Fig. 7 and Fig. 8. The particle history was set to $5.0\times10^8$ source particles, producing tally uncertainty of $7.0\times10^{-3}$ for the F4, a range of $1.0\times10^{-4}$ to $1.0\times10^{-2}$ for the F5, and $1.0\times10^{-4}$ for the F6 tallies. While the plotted spectra do have error bars, they are smaller than the displayed symbol. The random number generator was set to the 4th version, with a seed value of 2147483647 and a stride value of 11973779.

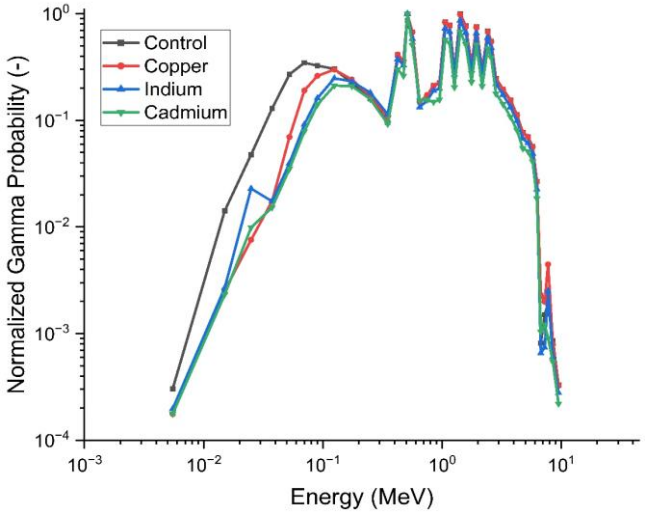


Fig. 5 Comparison of MCNP generated gamma spectra in the drop tube location for the selected metals.

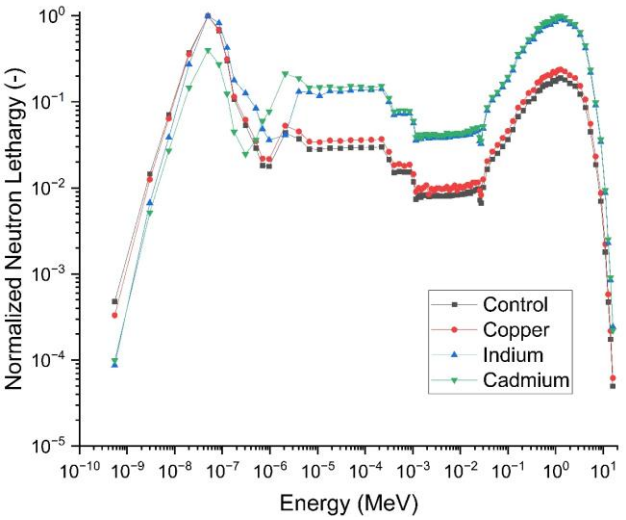


Fig. 6 Comparison of MCNP generated neutron spectra in the drop tube location for the selected metals.

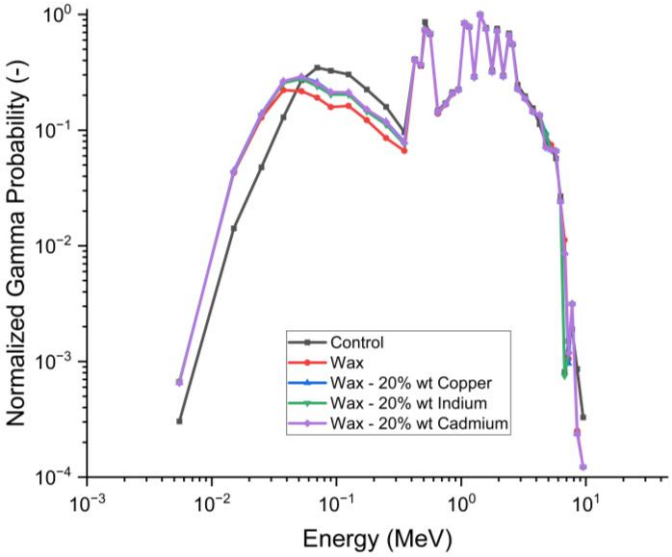


Fig. 7 comparison of MCNP generated gamma spectra in the drop tube location for 20% weight of the selected metals suspended in wax.

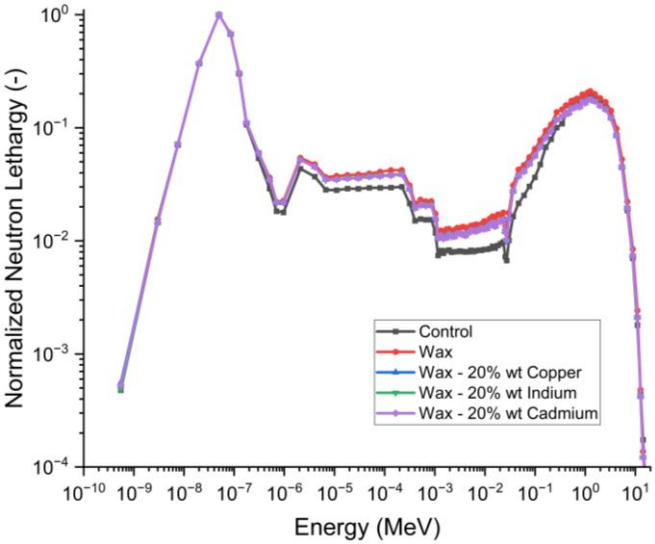


Fig. 8 comparison of MCNP generated neutron spectra in the drop tube location for 20% weight of the selected metals suspended in wax.

## VI. Dosimetry

The thermoluminescent dosimeter is a standardized means of collecting the dose of a radiation environment. While there are different types of TLDs, the operation is uniform across materials. Lithium-fluoride (LiF) type TLDs are special in that the Li-6 isotope has an incredibly high affinity for neutrons *via* the (n,α) reaction relative to the Li-7 isotope. By manufacturing TLDs using different ratios of the isotopes, two types of dosimeters can be developed. Where a TLD-600 is sensitive to neutrons and gammas, and a TLD-700 is only sensitive to gammas. When used in tandem, these two TLDs can determine the dose contribution from gammas and neutrons separately. Thus, the TLD 600/700 pair is an ideal dosimeter for the fission environment, such that the LiF crystals are large enough to prevent charge saturation [25]. Fig. 9 displays the neutron cross-sections for both isotopes of lithium. Similar to neutrons, gamma interaction with LiF is a function of energy, but is dependent upon density as opposed to isotope. The NIST photon attenuation for LiF can be found in Fig. 10.

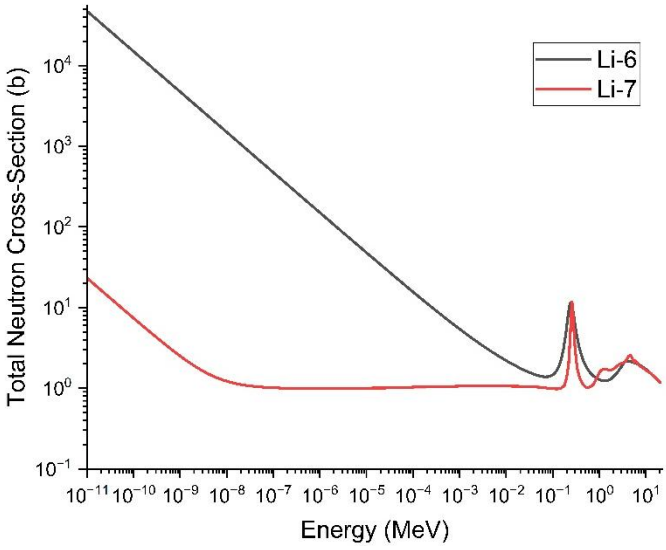


Fig. 9 ENDF/B-VIII.0 total neutron cross-section for Li-6 and Li-7 [26], [27].

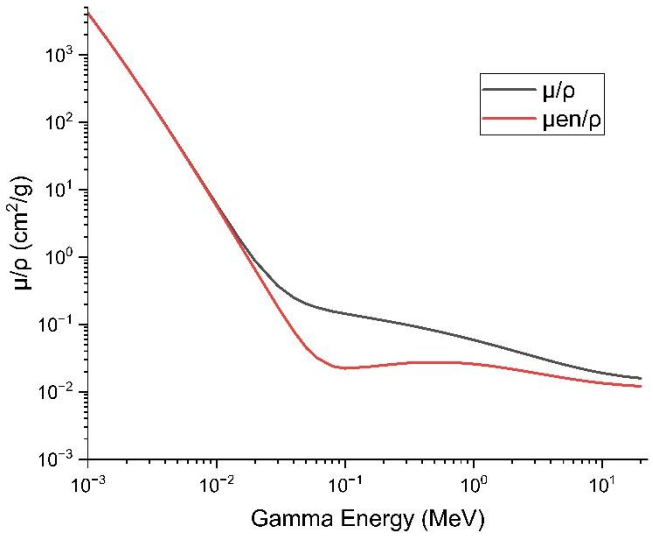


Fig. 10 NIST photon attenuation for lithium fluoride TLDs [28].

The data for both neutron and gamma interactions with the TLDs can be used for the development of energy correction factors. The relationship can be solved analytically or through MCNP. Due to the complex nature of geometry and energy spectrum found within most fission fields, Monte Carlo methods are preferred. The gamma energy relation is simpler to develop because it is not strongly correlated with the radiation field geometry and can be applied universally. It is also normalized to cobalt-60, which is typically used as the calibration source. Fig. 11 shows the MCNP-generated energy correction factors for both TLD-600/700. It should be noted that the response between the isotopes is nearly identical. Furthermore, in a complex gamma field, the corrections can be applied by determining the average gamma energy of the spectrum.

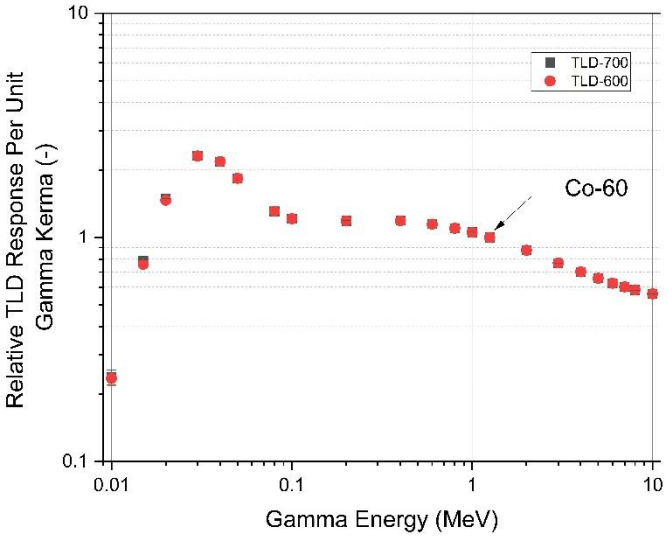


Fig. 11 MCNP generated lithium fluoride TLD gamma energy correction factors for TLD-600 and TLD-700.

A similar process can be applied to the neutrons; however, what must be considered is the change in the spectrum hardness compared to the initial spectrum. A monoenergetic input cannot be used to build the model in a system with a strong moderator. This is due to the neutrons interacting with a medium and forming a spectrum regardless of the initial monoenergetic condition. Therefore, a complete shift in the neutron energy spectrum is required as the MCNP input. One assumption that was made for this work is that there is no spectral reshaping, only energy shifting. As shown in the previous section, there is strong evidence for spectral reshaping. This shifts the neutrons towards a more thermal distribution. Without advanced spectrum unfolding techniques, it is difficult to estimate how much the thermal peak changes relative to the initial energy spectrum. This model assumes a normalized Watt-fission spectrum for U-235 shown in Fig. 3, then applies a shifting factor to the energies while maintaining the probability of each energy. The results for both the TLD-600/700 response to the energy shift can be found in Fig. 12 and Fig. 13, respectively. It is proposed that the use of bare and cadmium covered foils to determine the cadmium ratio can be used to approximate the spectrum shift. Of note, this practice only considers thermal and epithermal neutrons. The In-115(n,n')In-115m1 reaction can be used to isolate the fast neutrons if the flux is high enough. Alternatively, a method was described in 1958 by placing indium foils within a sphere of paraffin, followed by a sheet of cadmium. The principle idea is to allow only fast and epithermal neutrons to pass through the foils, subsequently thermalizing the flux for the In-115(n,γ)In-116m2 reaction [29].

Following the dose-to-charge correlation, the gamma and neutron dose in the mixed field can be determined using equations (11) and (12). Where $D_n$ is the neutron dose, $D_\gamma$ is the gamma dose, $D_{0/600}$ is the charge correlated dose for the TLD-600, $D_{0/700}$ is the charge correlated dose for the TLD-700, and $K_n$ and $K_\gamma$ are the energy corrections for neutrons and gammas, respectively.

$$D_\gamma = D_{0/700} K_\gamma \tag{11}$$

$$D_n = D_{0/600} K_n - D_\gamma \tag{12}$$

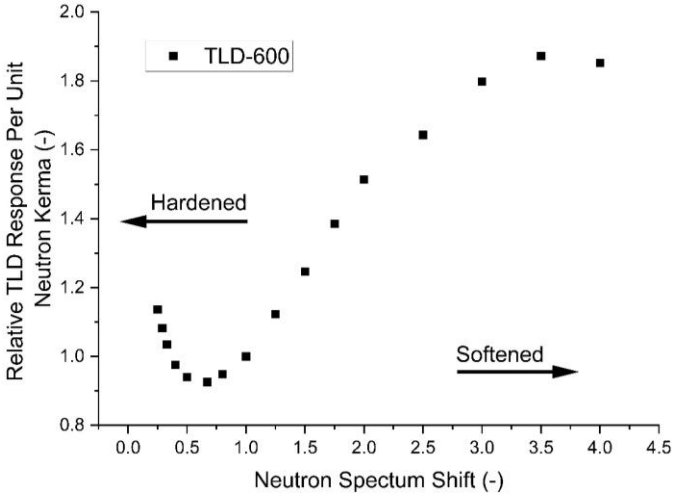


Fig. 12 MCNP generated TLD-600 energy correction factors as a function of neutron spectrum hardening. Note that both abscissa and ordinate are now linear scale.

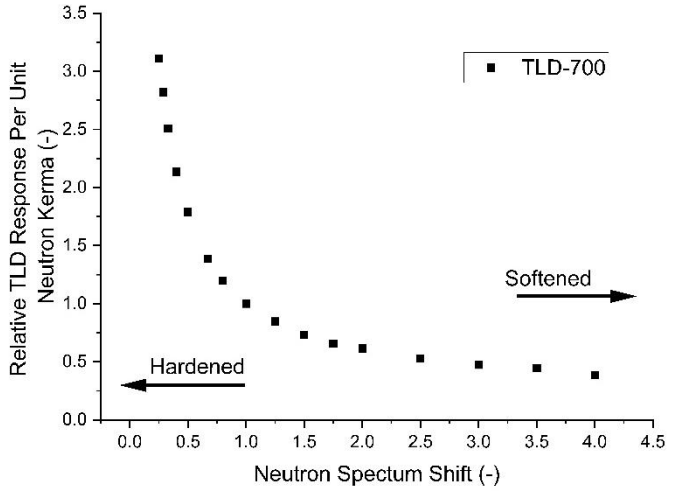


Fig. 13 MCNP generated TLD-700 energy correction factors as a function of neutron spectrum hardening. Note that both abscissa and ordinate are now linear scale.

Once the values for neutron and gamma dose are determined for the environment, they must be corrected for the medium in which the dose is of interest. Several theories are well established in dosimetry literature, but the Bragg-Gray cavity theory is sufficient for the scale of the targets placed within the fission spectrum for this report [30]. The assumptions for the Bragg-Gray theory are such that there is a charged particle equilibrium, all electrons causing ionizations are from the phantom material, the secondary electron energy spectrum is unchanged, and all electrons are deposited locally. Similar to the gamma condition above, an average energy for the spectrum can be assumed. Equation (13) can then be used to relate the dose in the TLD to the target material. Where, $\mu_{en}/\rho$ is the mass energy-absorption coefficient ratio between the materials for the average energy of the gamma field. These values are well documented by NIST.

$$\frac{D_{Medium}}{D_{LiF}} = \left(\frac{\mu_{en}}{\rho}\right)_{LiF}^{Medium} \tag{13}$$

The use of cavity theory is necessary to prevent under/over estimating the dose in any particular test material. However, the

true benefit is for a characterization of the environment relative to the TLD in which other non-silicon materials can be tested without the need for reestablishing the energy dependent dose for any given test casing. This minimizes the risk for creating unnecessary activated material.

## VII. Systematic Approach From First Principles

The materials selection remains only half of the challenge when designing test casings and conformal coatings for a gamma-producing medium. The physical dimensions of the material must optimize three material properties to achieve maximum gamma yield at the testing location. The first is a large cross-section for absorption, though this was already accounted for in the material selection. The second is neutron scattering, specifically the average logarithmic energy decrement per collision ($\xi$). It is of interest to thermalize neutrons, but not prematurely absorb low-energy neutrons. Finally, the linear mass attenuation of the conversion material must be such that it transmits photons of energies produced from the capture reactions. External to the material, the neutron spectrum and flux directly affect the thickness of the conversion layer. While the complete neutron energy spectrum need not be defined, the relative ratio of fast to thermal flux should be estimated. One final limitation, at least in the case of PUR-1, is the space available for the test casing. The 7.6 cm drop tube constrains the thickness of any shielding layer placed between the tube wall and the DUT. To address this, four designs are considered: an unconstrained layered design using wax followed by a metal sheet, an unconstrained mixture of wax and powdered metal at 20% by weight, a space-limited layered design, and a metal sheet alone with no wax.

Considering the first design, a layer of wax (converter A) will be used to thermalize epithermal neutrons and higher. The optimal length balances thermal neutron production with thermal neutron absorption. Then the metal layer (converter B) will be placed for the conversion of neutrons to gammas, balancing gamma production and attenuation.

Equation (14) describes the fast neutron flux loss following an exponential attenuation due to scattering and removal processes.

$$\frac{d\phi_f(x)}{dx} = -k_A\phi_f(x) \Longrightarrow \phi_f(x) = \phi_{f,0}e^{-k_A x} \tag{14}$$

Where $\phi_{f,0}$ is the initial incident fast neutron flux and $k_A$ is an effective fast-to-thermal conversion coefficient defined as in equation (15).

$$k_A = \frac{\xi\Sigma_s}{ln(E_0/E_{th})} \tag{15}$$

Where $\xi$ is the average logarithmic energy decrement per collision, $\Sigma_s$ is the macroscopic scattering cross section of converter A, $E_0$ is the average incident fast neutron energy, and $E_{th}$ is the thermal neutron energy.

Thermal neutrons are produced via down-scattering of fast neutrons and are lost through absorption and leakage. The thermal neutron flux $\phi_{th}(x)$ satisfies equation (16).

$$\frac{d\phi_{th}(x)}{dx} = k_A\phi_f(x) - a_A\phi_{th}(x) \tag{16}$$

where the effective thermal loss coefficient is shown in equation (17).

$$a_A = \Sigma_{a,th} + \alpha_{leak} \tag{17}$$

Where $\Sigma_{a,th}$ is the macroscopic thermal absorption cross section, and the leakage term is modeled using a diffusion-inspired approximation shown in (18).

$$\alpha_{\text{leak}} = DB^2, D = \frac{1}{3\Sigma_{tr}} \tag{18}$$

with $D$ the diffusion coefficient, $\Sigma_{tr}$ the macroscopic transport cross section, and $B^2$ the geometric buckling. Solving the coupled fast–thermal system yields the thermal neutron flux exiting converter A, which serves as the incident thermal flux into converter B, shown in equation (19).

$$\phi_{th}^{B,in}(L_A) = \phi_{th,0}e^{-a_A L_A} + \phi_{f,0}\frac{k_A}{a_A - k_A}(e^{-k_A L_A} - e^{-a_A L_A}) \tag{19}$$

Defining the fast-to-thermal flux ratio at the entrance as equation (20).

$$r = \frac{\phi_{f,0}}{\phi_{th,0}} \tag{20}$$

The optimal converter thickness that maximizes the thermal neutron flux at the exit of converter A is shown in equation (21).

$$\frac{d\phi_{th}^{B,in}(L_A)}{dL_A} = 0 \Longrightarrow L_{A,opt} = \frac{1}{a_A - k_A} ln\left(\frac{a_A(k_A(r+1) - a_A)}{r k_A^2}\right) \tag{21}$$

Subject to constraint in equation (22)

$$k_A(r+1) - a_A > 0 \tag{22}$$

The performance of converter A is quantified using a normalized figure of merit. The figure of merit for converter A is provided by equation (23).

$$FOM_A = \frac{\phi_{th}^{B,in}(L_A)}{\phi_{th,0}} \tag{23}$$

The FOM is maximized at $L_{A,\,opt}$. This term captures the efficiency of converting incident fast and thermal neutrons into useful thermal neutrons delivered to converter B. Converter B is designed to capture thermal neutrons and emit prompt gamma rays that escape toward the silicon target.

The thermal neutron flux in converter B decays exponentially due to neutron capture by way of equation (24)

$$\phi_{th}^{B}(x) = \phi_{th}^{B,in}e^{-\Sigma_{c,B}x} \tag{24}$$

where $\Sigma_{c,B}$ is the macroscopic thermal neutron capture cross section of converter B.

A prompt gamma ray is produced at depth $x$ must traverse a distance $L_B - x$ to escape the converter. The escape probability is provided in equation (25).

$$P_{esc}(x) = e^{-\mu_B(L-x)} \tag{25}$$

where $\mu_B$ is the linear gamma attenuation coefficient of converter B evaluated at the dominant prompt gamma energy. The gamma current exiting converter B is obtained by integrating the local capture rate weighted by the escape probability shown in equation (26).

$$J_\gamma(L_B) = \phi_{th}^{B}\Sigma_{c,B}I_\gamma\int_0^L P_{esc}(x)dx\,\phi_{th}^{B,in}\Sigma_{c,B}I_\gamma\int_0^L e^{-\Sigma_{c,B}x}e^{-\mu_B(L-x)}dx \tag{26}$$

Evaluating the integral yields in equation (27).

$$J_\gamma(L_B) = \phi_{th}^{B,in}\Sigma_{c,B}I_\gamma\frac{e^{-\mu_B L_B} - e^{-\Sigma_{c,B}L_B}}{\Sigma_{c,B} - \mu_B} \tag{27}$$

Maximizing the gamma current with respect to $L_B$ gives the optimal thickness in equation (28).

$$L_{B,opt} = \frac{1}{\Sigma_{c,B} - \mu_B}\ln\left(\frac{\Sigma_{c,B}}{\mu_B}\right) \tag{28}$$

The figure of merit for converter B is in equation (29).

$$FOM_B = \Sigma_{c,B} I_\gamma \frac{e^{-\mu_B L_B} - e^{-\Sigma_{c,B} L_B}}{\Sigma_{c,B} - \mu_B} \quad (29)$$

The total performance of the layered converter is provided in equation (30).

$$FOM_{total} = FOM_A \cdot FOM_B \cdot E_\gamma \cdot \left(\frac{\mu_{en}}{\rho}\right)_{Si} \quad (30)$$

where $E_\gamma$ is the prompt gamma energy and $(\mu_{en}/\rho)_{\mathrm{Si}}$ is the mass energy-absorption coefficient of silicon at that energy. This expression is proportional to the gamma-induced dose rate in silicon per unit incident thermal neutron flux. The total optimal thickness of the layered converter is therefore the optimal length of the layered design becomes equation (31).

$$L_{total,opt} = L_{A,opt} + L_{B,opt} \quad (31)$$

A similar analysis can be performed for the wax and metal powder type design. For the fast neutron flux $\phi_f(x)$ in the mixture is modeled as exponential attenuation in equation (32).

$$\phi_f(x) = \phi_{f,0} e^{-k_m x} \quad (32)$$

Where $\phi_{f,0}$ is the incident fast neutron flux at $x = 0$, and $k_m = (1-f)k_A$ is an effective fast-to-thermal conversion/removal coefficient of the mixture [$\mathrm{cm}^{-1}$] (analogous to $k_A$ in the layered case) with f the volume fraction of component B. The thermal neutrons are produced by down-scattering of the fast flux and are lost through thermal absorption and leakage. The resulting thermal flux at the thickness $L$ is shown in equation (33).

$$\phi_{th}(L) = \phi_{th,0} e^{-a_m L} + \phi_{f,0} \frac{k_m}{a_m - k_m} (e^{-k_m L} - e^{-a_m L}) \quad (33)$$

Where $\phi_{th,0}$ is the incident thermal neutron flux at $x = 0$, and $a_m$ is the effective thermal loss coefficient of the mixture provided by equation (34)

$$a_m = \Sigma_{a,th,\mathrm{mix}} + \alpha_{\mathrm{leak,mix}},\ \alpha_{\mathrm{leak,mix}} = D_{\mathrm{mix}} B^2, D_{\mathrm{mix}} = \frac{1}{\Sigma_{tr,\mathrm{mix}}} \quad (34)$$

With $\Sigma_{a,th,\mathrm{mix}} = (1-f)\Sigma_{a,A} + f\Sigma_{a,B}$. The entrance fast-to-thermal ratio r is defined similarly to the layered converter case. Thermal neutron capture in the mixture produces prompt gammas. If the macroscopic capture cross-section is $\Sigma_{c,\mathrm{mix}} = f\Sigma_{c,\mathrm{B}}$, and the prompt gamma yield (highest-intensity line only) is $I_\gamma$, then the escaping gamma current from the exit face at $x = L$ is shown in equation (35).

$$J_\gamma(L) = \Sigma_{c,mix} I_\gamma \int_0^L \phi_{th}(x) e^{-\mu_m (L-x)} dx \quad (35)$$

where $e^{-\mu_m(L-x)}$ is the escape probability for a gamma produced at depth $x$, and $\mu_m = (1-f)\mu_A + f\mu_B$, is the linear gamma attenuation coefficient of the mixture evaluated at the dominant prompt gamma energy. Carrying out the integral produces equation (36).

$$J_\gamma(L) = \Sigma_{c,mix} I_\gamma \left[\phi_{th,0} \frac{e^{-\mu_m L} - e^{-a_m L}}{a_m - \mu_m} + \phi_{f,0} \frac{k_m}{a_m - k_m} \left(\frac{e^{-\mu_m L} - e^{-k_m L}}{k_m - \mu_m} - \frac{e^{-\mu_m L} - e^{-a_m L}}{a_m - \mu_m}\right)\right] \quad (36)$$

This expression captures the competing effects of (i) increased thermal production and capture volume with increasing $L$ and (ii) self-attenuation of prompt gammas as $L$increases. The mixture converter figure of merit is defined to be proportional to silicon dose rate via the emitted gamma energy and silicon energy absorption from equation (37).

$$FOM_{mix} = J_\gamma(L) \cdot E_\gamma \cdot \left(\frac{\mu_{en}}{\rho}\right)_{Si} \quad (37)$$

Where $E_\gamma$ is the dominant prompt gamma energy and $(\mu_{en}/\rho)_{\mathrm{Si}}$ is the mass energy-absorption coefficient of silicon at $E_\gamma$. The optimal mixture thickness $L_{\mathrm{mix,opt}}$ is obtained by equation (38).

$$\frac{d\,\mathrm{FOM_{mix}}}{dL} = 0 \Leftrightarrow \frac{dJ_\gamma(L)}{dL} = 0 \quad (38)$$

which can be solved numerically since $J_\gamma(L)$ contains multiple exponential terms with different attenuation constants ($k_m$, $a_m$, $\mu_m$).

## VIII. MCNP Energy Deposition

While the shift in the gamma and neutron spectrum is relevant for understanding the radiation environment, the energy deposited in the device under test is the value of importance for evaluating the effectiveness of energy tuning for the casing material used external to a test device. The use of neutron and photon tracking F6 tallies provides this insight. The energy deposition per source particle is provided in Fig. 14. It is important to note, that the values below do not contain the optimal thickness values, rather the metal sheets are 0.7 mm to provide a direct comparison with the optimal thickness of cadmium. Whereas, the thickness of the wax models is 0.2 cm. This value is somewhat arbitrary, but was selected to attempt to recreate the same volume of metal present in the casing while adhering to the space limitation of the PLA container. The optimal thickness of cadmium was determined through the algorithm described above.

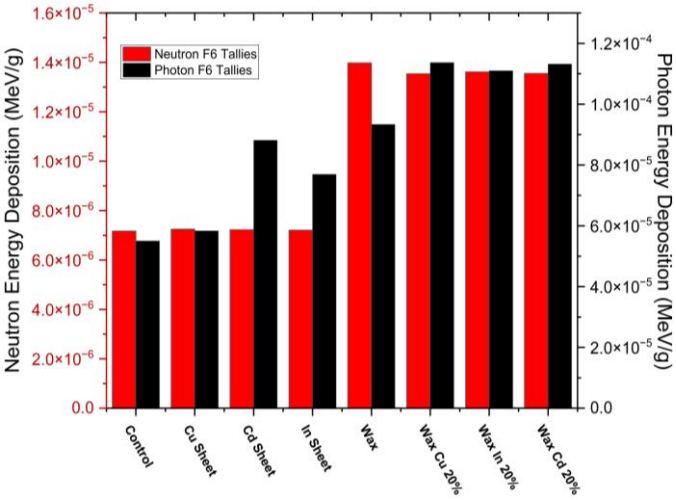


Fig. 14 MCNP generated F6 energy deposition into silicon for the selected materials in the PUR-1 drop tube.

The values of the selected materials can then be compared to the controlled environment as a percent difference. Ultimately, providing insight to the contribution of the material *via* the prompt (n,γ) reaction. One critical distinction that must be made is that these results do not consider the time effects of irradiating the material, thus the delayed gammas are not considered. The copper plays the largest role in the activation as the half-life for the activated Cu-66 is 5.12 minutes. This is long enough to be considered delayed, but short enough on the time span of a radiation test to contribute to the dose. Table I provides the relative change in photon and neutron energy deposition into silicon compared to the control PUR-1 drop tube environment.

TABLE I
RELATIVE CHANGE IN ENERGY DEPOSITED INTO SILICON

| Material | Relative Neutron Change (%) | Relative Photon Change (%) |
|---|---|---|
| Copper | 1.09 | 6.02 |
| Indium | 0.52 | 39.87 |
| Cadmium | 0.76 | 60.22 |
| Wax | 94.99 | 69.72 |
| Wax – Cu | 88.87 | 106.65 |
| Wax – In | 89.91 | 101.83 |
| Wax – Cd | 89.05 | 105.81 |

## IX. DISCUSSION

Neutron and gamma facilities used to qualify electronics as radiation hardened are in short demand and are often incredibly expensive compared to the remaining project's budget expenses. Thermal research reactors, such as PUR-1, offer accessible radiation environments but are limited for microelectronics testing. This is due to their highly moderated neutron spectra and relatively low gamma dose rates. As a result, they do not replicate the cobalt-60 conditions prescribed by MIL-STD-750D. This work addresses this gap by demonstrating that spectrum-tuning materials can substantially increase gamma deposition in silicon within a thermal reactor environment.

The MCNP6.3 simulations indicate that paraffin wax loaded with high cross-section metals may produce a large gain in gamma energy deposition when compared to the controlled environment. While metal sheets of cadmium and indium provide 39% - 60% increases in photon dose relative to the bare PUR-1 drop tube spectrum, the wax-metal composites generate up to 106% greater gamma energy deposition in silicon. This behavior arises from the combined effects of strong neutron moderation in wax, which increases the fraction of neutrons near the resonance and thermal regions where Cd-113, In-115, and Cu-63/65 exhibit large (n,γ) cross-sections, and the reduced self-shielding in the lower-density composite. The resulting capture gammas, many in the 0.01-0.1 MeV energy range where silicon's mass-energy absorption coefficient is highest, transmit efficiently through the composite and deposit energy more effectively than in the metal-sheet test casings.

The magnitude of this enhancement suggests that thermal reactors can be practical, low-cost platforms for preliminary microelectronics screening. By providing higher energy TID without modifying reactor hardware, these composites enable earlier radiation-response characterization and reduce reliance on high-cost, long-lead-time facilities such as WSMR FBR or ATHENA at NIF. Such early insight is especially valuable for commercial-off-the-shelf devices, which often fail late-stage qualification.

Limitations remain in the MCNP, such that the present model does not incorporate time-dependent activation products, spatial dose nonuniformities, or potential inhomogeneities within cast wax. Copper and indium activation may yield additional delayed gamma contributions that exceed the prompt-only predictions. Experimental foil activation, TLD 600/700 dosimetry, and high-resolution spectroscopy will be required to validate the simulated spectral shifts and quantify absolute dose enhancement. Future work will also evaluate casting methods to ensure uniform metal dispersion and apply spectrum-unfolding techniques to better resolve thermal and epithermal neutron behavior.

## X. CONCLUSION

This work demonstrates the possibility for thermal reactor facilities to help alleviate the limited availability of large-scale radiation testing facilities such as the National Ignition Facility or the White Sands Missile Range Fast Burst Reactor. While a radiation test within a thermal reactor cannot replace the qualification standards set forth in the MIL-STD-750D document, it may offer a supplemental method that can be conducted more frequent and earlier in the design process for a system that requires a radiation hardened designation.

MCNP6.3 code indicates that the use of copper, indium, and cadmium metal sheets or the same metals in powdered form deposited into wax can increase the gamma yield *via* the (n,γ) reaction. Where simulations of composite wax casings increase the deposited gamma energy by up to 106% when compared to the bare PUR-1 fission environment.

These results justify future work designing an experiment in PUR-1 that verifies the MCNP output. Where metal foil activation and spectrum unfolding techniques can be used to confirm the neutron spectrum shifts. High resolution scintillation detectors may aid in the development of photon energy spectra in the environment. Finally, pairs of TLD600/700 dosimeters combined with cavity theory can be used to validate the energy deposited into silicon from the modified neutron and gamma environment. Additional work will also address material homogeneity within wax composites and explore time-dependent activation effects. Together, these efforts will further advance the development of tunable fission-spectrum environments for microelectronics survivability testing.

### DISCLAIMER

The views expressed are those of the authors and do not reflect the official guidance or position of the United States Government, the Department of Defense the United States Air Force or the United States Space Force.

### ACKNOWLEDGMENT

This work heavily relies on the efforts of Major David Fobar, Major Adam Card, and LTC Andrew Decker of the Nuclear Science & Engineering Research Center at West Point, New York. True Miller and Brian Jowers III of the PUR-1 Research facility have been instrumental in gathering data. Also of Note, Dr. Linda Nie, Nathan Claus and Purdue's Environmental Health and Safety team for dosimetry preparation.

### REFERENCES AND FOOTNOTES

[1] E. National Academies of Sciences, *Testing at the Speed of Light: The State of U. S. Electronic Parts Space Radiation Testing Infrastructure*. Washington, D.C: National Academies Press, 2018.

[2] "Test Methods For Semiconductor Devices." Department of Defense, Feb. 23, 1983. [Online]. Available: https://www.navsea.navy.mil/Portals/103/Documents/NSWC_Crane/SD-18/Test%20Methods/MILSTD750.pdf

[3] M. Niichel *et al.*, “Design and Characterization of the Modified Purdue Subcritical Pile for Nuclear Research Applications,” Apr. 12, 2025, *Engineering*. doi: 10.20944/preprints202502.0812.v2.

[4] M. Niichel, T. Miller, B. Jowers, R. Cooper, and S. Chatzidakis, “Response of Boost Converters Under Fission-Spectrum Neutron and Gamma Radiation,” Aug. 13, 2025. doi: 10.31224/5057.

[5] M. Niichel and S. Chatzidakis, “Methodology For the Evaluation of Critical Components of the Scatterable Radiation Monitor Under Radiation Fields,” 2025, *arXiv*. doi: 10.48550/ARXIV.2503.08754.

[6] “Standard Guide for Selection and Use of Neutron-Activation Foils for Determining Neutron Spectra Employed in Radiation-Hardness Testing of Electronics.” Accessed: Nov. 14, 2024. [Online]. Available: https://www.astm.org/e0720-94.html

[7] American Society for Testing and Materials, “Standard Practice for Application of Thermoluminescence-Dosimetry (TLD) Systems for Determining Absorbed Dose in Radiation-Hardness Testing of Electronic Devices.” Aug. 06, 2020. [Online]. Available: https://compass.astm.org/content-access?contentCode=ASTM%7CE0668-20%7Cen-US

[8] J. E. Bevins *et al.*, “Performance evaluation of an energy tuning assembly for neutron spectral shaping,” *Nuclear Instruments and Methods in Physics Research Section A: Accelerators, Spectrometers, Detectors and Associated Equipment*, vol. 923, pp. 79–87, Apr. 2019, doi: 10.1016/j.nima.2019.01.049.

[9] E10 Committee, *Practice for Characterizing Neutron Fluence Spectra in Terms of an Equivalent Monoenergetic Neutron Fluence for Radiation-Hardness Testing of Electronics*. doi: 10.1520/E0722-19.

[10] K. Russell DePriest, “Historical Examination of the ASTM Standard E722 1-MeV Silicon Equivalent Fluence Metric,” Sandia National Laboratories, Albuquerque, NM, SAND2019-15194, 2019. [Online]. Available: https://www.osti.gov/servlets/purl/1592863

[11] James Edward Bevins, “Targeted Modification of Neutron Energy Spectra for National Security Applications,” University of California, Berkeley, CA, 2017.

[12] Wade Kloppenburg, “Neutron Spectral Effect on Microelectronic Device Performance,” Air Force Institute of Technology, AFIT-ENG-MS-20-90210, 2022. [Online]. Available: https://apps.dtic.mil/sti/html/trecms/AD1176801/

[13] A. Koning, M. Chadwick, and Hetrick, “Copper 65 neutron total cross-section.” ENDF/B-VIII.0, 2016.

[14] A. Koning, M. Chadwick, and Hetrick, “Copper 63 neutron total cross-section.” ENDF/B-VIII.0, 2016.

[15] W.G. Mughabghab, “Cadmium 113 neutron total cross-section.” ENDF/B-VIII.0, 2010.

[16] W.G. Mughabghab, “Indium 115 neutron total cross-section data.” Mar. 08, 2024. [Online]. Available: https://www-nds.iaea.org/exfor/servlet/X4sShowData?db=x4&op=get_plotdata&req=-1&ii=42&File=E4R10339_e4.zvd.dat.txt

[17] True Miller, “Production of Lutetium-177 Via the Indirect Route Using PUR-1,” Purdue University, West Lafayette, IN, 2021. [Online]. Available: https://www.proquest.com/docview/2838332159?pq-origsite=gscholar&fromopenview=true&sourcetype=Dissertations%20&%20Theses

[18] Clive Townsend, “Technical Specifications For the Purdue University Reactor, PUR-1,” Purdue University, 50–182, 2018.

[19] Jerome Verbeke, Chris Hagmann, and Doug Wright, “Simulation of Neutron and Gamma Ray Emission from Fission,” Lawrence Livermore National Laborator, UCRL-AR-228518, 2010.

[20] M. Hricova, M. Petkova, Z. Tomcikova, and A. Ujhelyiova, “The Effect of Inorganic Pigments on the Rheological Properties of the Color Masterbatches from Polylactic Acid,” *Fibers*, vol. 13, no. 9, p. 122, Sept. 2025, doi: 10.3390/fib13090122.

[21] Shannon Murray, Elizabeth Jones, Caroline Winters, Abraham Ramirez, and Seth Davis, “Exploring the process-structureproperty relationship of Aerosol Deposition to phosphor coatings for non-contact thermometry,” Sandia National Laboratories, Albuquerque, NM, SAND2023-13163, 2023. [Online]. Available: https://www.osti.gov/servlets/purl/2430299

[22] C. Ma and A. E. Nahum, “Bragg-Gray theory and ion chamber dosimetry for photon beams,” *Phys. Med. Biol.*, vol. 36, no. 4, pp. 413–428, Apr. 1991, doi: 10.1088/0031-9155/36/4/001.

[23] R. Côté, M. Azzouni, and V. Demers, “Impact of binder constituents on the moldability of titanium-based feedstocks used in low-pressure powder injection molding,” *Powder Technology*, vol. 381, pp. 255–268, Mar. 2021, doi: 10.1016/j.powtec.2020.12.008.

[24] Mahdi Hadi Jasim and Naji Talib Abdulameer, “Neutron capture cross section measurements of paraffin wax,” *International Journal of Application or Innovation in Engineering & Management*, vol. 3, no. 4, Apr. 2014.

[25] G. F. Knoll, *Radiation detection and measurement*, 4th ed. Hoboken, N.J: John Wiley, 2010.

[26] G.M. Hale, “Neutron Total Cross Section Li-6(N,Tot).” ENDF/B-VIII.0. [Online]. Available: https://www-nds.iaea.org/exfor/servlet/E4sGetTabSect?sum=1&SectID=8943039&req=2983

[27] P.G. Young, “Neutron total cross sections. Li-7 (N,TOT).” ENDF/B-VIII.0, Aug. 1988. [Online]. Available: https://www-nds.iaea.org/exfor/servlet/E4sGetTabSect?sum=1&SectID=8943120&req=2982

[28] National Institue of Standards and Technology, “Lithium Fluoride Xray Mass Coefficient.” [Online]. Available: https://physics.nist.gov/PhysRefData/XrayMassCoef/ComTab/lithiumflu.html

[29] Lloyd D. Stephens and Alan R. Smith, “Fast-Neutron Surveys Using Indium Foil Activation,” University of California, Berkeley, CA, 1958.

[30] L. V. Spencer and F. H. Attix, “A Theory of Cavity Ionization,” *Radiation Research*, vol. 3, no. 3, p. 239, Nov. 1955, doi: 10.2307/3570326.